ELSEVIER

Biophysical Chemistry 126 (2007) 86–93

Biophysical Chemistry

http://www.elsevier.com/locate/biophyschem

Structure of a novel *N*-acetyl-L-citrulline deacetylase from *Xanthomonas campestris*

Dashuang Shi [a,*], Xiaolin Yu [a], Lauren Roth [b], Mendel Tuchman [a], Norma M. Allewell [b]

[a] *Children's Research Institute, Children's National Medical Center, 111 Michigan Avenue, N.W., Washington, D.C. 20010-2970, USA*
[b] *College of Chemical and Life Sciences, 2300 Symons Hall, University of Maryland, College Park, MD 20742, USA*

Received 10 February 2006; accepted 10 May 2006
Available online 5 June 2006

Abstract

The structure of a novel acetylcitrulline deacetylase from the plant pathogen *Xanthomonas campestris* has been solved by multiple-wavelength anomalous dispersion (MAD) using crystals grown from selenomethionine-substituted protein and refined at 1.75 Å resolution. The asymmetric unit of the crystal contains one monomer consisting of two domains, a catalytic domain and a dimerization domain. The catalytic domain is able to bind a single Co(II) ion at the active site with no change in conformation. The dimerization domain forms an interface between two monomers related by a crystallographic two-fold symmetry axis. The interface is maintained by hydrophobic interactions between helices and hydrogen bonding between two β strands that form a continuous β sheet across the dimer interface. Because the dimers are also related by two-fold crystallographic axes, they pack together across the crystal via the dimerization domain, suggesting that higher order oligomers may form in solution. The polypeptide fold of the monomer is similar to the fold of *Pseudomonas* sp. carboxypeptidase G2 and *Neisseria meningitidis* succinyl diaminopimelate desuccinylase. Structural comparison among these enzymes allowed modeling of substrate binding and suggests a possible catalytic mechanism, in which Glu130 functions as a bifunctional general acid–base catalyst and the metal ion polarizes the carbonyl of the acetyl group.

Keywords: ArgE gene; Deacetylase; *N*-acetyl-L-citrulline; *N*-acetyl-L-ornithine; Arginine biosynthesis; Crystal structure

1. Introduction

The first five steps of the canonical arginine biosynthetic pathway in yeast, plants, and bacteria utilize acetylated substrates [1]. The first non-acetylated substrate is L-ornithine, produced from *N*-acetyl-L-ornithine in a reaction catalyzed by *N*-acetyl-L-ornithine deacetylase (AODase) [2–4]. Recently, a novel arginine biosynthetic pathway was identified in *Xanthomonas campestris*, a major plant pathogen, in which *N*-acetyl-L-ornithine is the substrate for the transcarbamoylation reaction and the product is *N*-acetyl-L-citrulline [5,6]. Thus, a second novel enzyme, *N*-acetylcitrulline deacetylase (ACDase) is required to catalyze the deacetylation of *N*-acetyl-L-citrulline to produce L-citrulline [6,7].

We have cloned, expressed, and determined crystal structures of *N*-acetyl-L-citrulline deacetylase from *X. campestris* in the metal-free form and with a single Co(II) ion bound at the active site. Binding of Co(II) was investigated because many deacetylases have been shown to require at least one metal ion for catalysis [8], although their role in catalysis is still not fully understood. The structures suggest a catalytic mechanism and provide new insights into how related enzymes discriminate among different substrates. They also provide a starting point for controlling the growth of *X. campestris* by designing specific inhibitors that selectively inactivate ACDase.

2. Experimental

2.1. Purification, crystallization, and data collection

Gene cloning, protein expression and purification, and data collection were described previously [7]. Briefly, the argE' gene

* Corresponding author. Tel.: +1 202 884 5817; fax: +1 202 884 6014.
E-mail address: dshi@cnmcresearch.org (D. Shi).

0301-4622/$ - see front matter © 2006 Elsevier B.V. All rights reserved.
doi:10.1016/j.bpc.2006.05.013

was PCR amplified from *X. campestris* genomic DNA (ATCC 3391D), cloned into a pET28a expression vector (Novagen). and expressed in *Escherichia coli* BL21(DE3) cells (Invitrogen). The protein was purified using Ni-affinity and DEAE columns (GE Healthcare). After thrombin digestion, the protein was separated from the his-tag by Ni-affinity chromatography, and concentrated to 12 mg/ml for crystallization trials. The metal-free protein was prepared by dialysis against a buffer containing 100 mM NaCl, 20 mM Tris–HCl pH 8.0, 1 mM EDTA and 5 mM β-mercaptoethanol, while Co(II)-bound protein was prepared by dialysis into a buffer containing 100 mM NaCl, 20 mM HEPES pH 8.0, and 200 mM $CoCl_2$. Crystals of metal-free native protein and selenomethionine-substituted protein grown from a solution containing 0.2 M magnesium formate, 12–15% (w/v) PEG 3350 pH 5.9 by hanging-drop vapor diffusion as reported previously [7]. The crystals of Co(II)-bound protein were grown from a solution containing 100 mM sodium acetate, 200 mM sodium formate pH 4.6.

High-resolution (1.75 Å) data for metal-free and the Co(II)-bound crystals were collected from a single frozen crystal cryoprotected by replacing the mother liquor with the reservoir solution supplemented by 20% (v/v) ethylene glycerol on beam line X26C at the Brookhaven National Laboratory. The crystals belong to space group *C*2 with unit cell parameters: $a=94.13$, $b=95.23$, $c=43.61$ Å, $\beta=93.76°$. Reasonable values for the packing density calculation suggested that there is one monomer in an asymmetrical unit [9]. High-resolution data (1.75 Å) for metal-free crystals soaked with 100 mM *N*-acetyl-L-citrulline or 100 mM *N*-acetyl-L-ornithine were also collected; however, the electron density maps provided no evidence of ligand binding.

High-resolution (1.75 Å) MAD data were also collected from a single frozen crystal of the selenomethionine-substituted protein on beam line X12B at Brookhaven National Laboratory. An X-ray excitation scan had an intense absorption edge at 12655 eV, characteristic of Se. The data were collected at three wavelengths on the Se absorption edge (0.9780 Å), inflection point (0.9761 Å) and in a low energy region remote from the absorption edge (0.9550 Å) [7]. The unit cell parameters for the selenomethionine-substituted crystals were similar to those of the metal-free native crystals. All diffraction data were processed using the HKL2000 package [10] and reduced using program TRUNCATE in the CCP4 suite [11].

2.2. Structure determination and refinement

The structure was solved using the MAD data [7]. Six selenium sites were found and refined using SOLVE [12], and 82% of the polypeptide chain was automatically traced using RESOLVE [13]. The model was manually completed using O [14].

CNS [15] was used to refine the 1.75 Å data sets collected on the metal-free and the Co(II)-bound crystals. Refinement of the metal-free structure converged with residuals $R=0.226$ and $R_{free}=0.258$. The residuals R and R_{free} for the Co(II)-bound structure were 0.198 and 0.224, respectively. 92.1% of the residues were in the most favored region of the Ramachandran plot calculated by program PROCHECK [16], with no residues in the disallowed region. Data collection and refinement statistics are summarized in Table 1. Coordinates for the metal-free and Co-bound structures have been deposited at the PDB with accession codes 2F8H and 2F7V, respectively.

2.3. Structural modeling of the substrate binding

Even though loop and helix positions are significantly different among ACDase structure and its closely related structures of succinyldiaminopimelate desuccinylase from *Neisseria meningitidis mc58*. (PDB ID: 1VGY) [17] and carboxypeptidase G2 from a *Pseudomonas* sp. (PDB ID: 1CG2) [18], their active sites are extremely similar. When the metal-binding residues of these structures are superimposed onto ACDase using the equivalent residues (His72, Asp103, Glu130–131, Glu155 and His340), the r.m.s. differences are only 0.21 and 0.46 Å, respectively. Similarly, the active site structure of ACDase is also similar to other bi-metal enzymes such as aminopeptidase from *Aeromonas proteolytica* [19].

Table 1
Data collection and refinement statistics for ACDase

	Data 1	Data 2
Protein buffer	20 mM Tris–HCl	20 mM HEPES
	pH 8.0	pH 8.0
	100 mM NaCl	100 mM NaCl
	1 mM EDTA	200 mM $CoCl_2$
Crystallization conditions	200 mM $MgCl_2$	100 mM Na acetate
	12–15% PEG 3350	200 mM Na formate
	pH 5.9	pH 4.6
Space group	*C*2	*C*2
Resolution (Å)	1.75	1.75
Unit-cell parameters	$a=94.13$ Å	$a=94.07$ Å
	$b=95.23$ Å	$b=95.43$ Å
	$c=43.61$ Å	$c=43.67$ Å
	$\beta=93.76°$	$\beta=93.76°$
Measurements	286,692	142,933
Unique reflections	37,941	38,233
Redundancy	7.6 (6.9)[a]	3.7 (3.5)
Completeness (%)	98.1 (96.0)	98.7 (97.0)
$\langle I/\sigma(I)\rangle$	22.3 (3.5)	18.4 (2.8)
R_{merg} (%)[b]	6.5 (39.7)	5.2 (35.5)
Wilson B (Å^2)	19.6	19.7
Resolution range (Å)	50–1.75	50–1.75
Number of protein atoms	2617	2698
Number of water atoms	353	370
Number of hetero-atoms	0	1
R_{msd} of bond lengths (Å)	0.005	0.005
R_{msd} of bond angle (°)	1.3	1.3
R_{work} (%)[c]	22.6	19.7
R_{free} (%)[d]	25.8	22.5
Average *B* factor (Å^2)	22.1	25.0

[a] Figures in brackets apply to the highest resolution shell.

[b] $R_{merg}=\sum_h\sum_i|I(h,i)-\langle I(h)\rangle|/\sum_h\sum_i I(h,i)$, where $I(h,i)$ is the intensity of the ith observation of reflection h, and $\langle I(h)\rangle$ is the average intensity of redundant measurements of reflection h.

[c] $R_{work}=\sum_h|F_{obs}-F_{calc}|/\sum_h F_{obs}$.

[d] $R_{free}=\sum_h|F_{obs}-F_{calc}|/\sum_h F_{obs}$ for 10% of the reserved reflections.

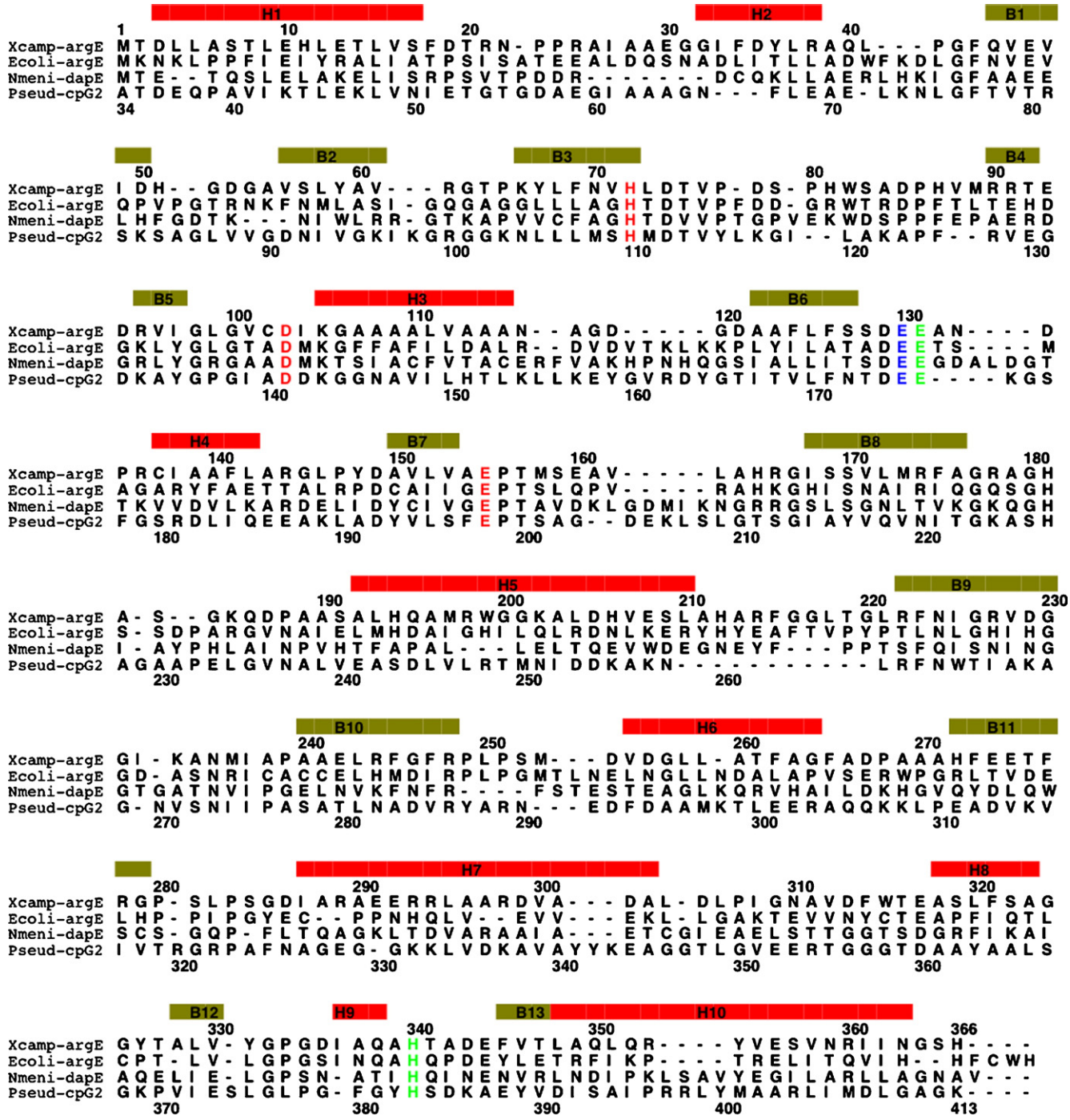

Fig. 1. Sequence alignment of *X.* campestris ACDase, *E.* coli AODase, *N. meningitidis* succinyl diaminopimelate desuccinylase and *Pseudomonas* sp. strain RS-16 carboxypeptidase G2. The secondary structural elements are indicated by boxes in yellow-green (β-strand) and red (α-helix) above the sequence. Residues that are involved in Co(II) binding are colored in red. The residues that are proposed to involve in substrate binding are colored green. Glu130 which is proposed to be the general acid–base catalyst is colored blue. The figure was drawn using program ALSCRIPT [26].

Therefore, all these structures can be used as a guide for modeling substrate binding of ACDase. The coordinates of *N*-acetyl-L-citrulline were taken from the structure of *N*-acetyl-L-ornithine transcarbamoylase complexed with *N*-acetyl-L-citrulline (PDB ID: 1YH1). The position and torsion angles of substrate were adjusted using O [14] to fit the substrate into the active site. Since the model is highly speculative, no energy minimization was carried out.

3. Results and discussion

3.1. Monomer structure

The refined model of the asymmetric unit, which consists of a single monomer, has 360 protein residues and 334 water molecules in the metal-free structure, and 360 protein residues, 370 water molecules and one Co(II) in the Co(II)-bound

Fig. 2. Structural comparison of ACDase (A), *N. meningitidis* mc58 succinyl diaminopimelate desuccinylase (B) and *Pseudomonas* sp. strain RS-16 carboxypeptidase G2 (C). Green arrows indicate segments that are hydrogen bonded to an adjacent strand, α-helices are red and β-sheets are green. The Co(II) ion in the active site is shown as a pink ball. The figures were drawn with MOLSCRIPT [27] and Raster3D [28].

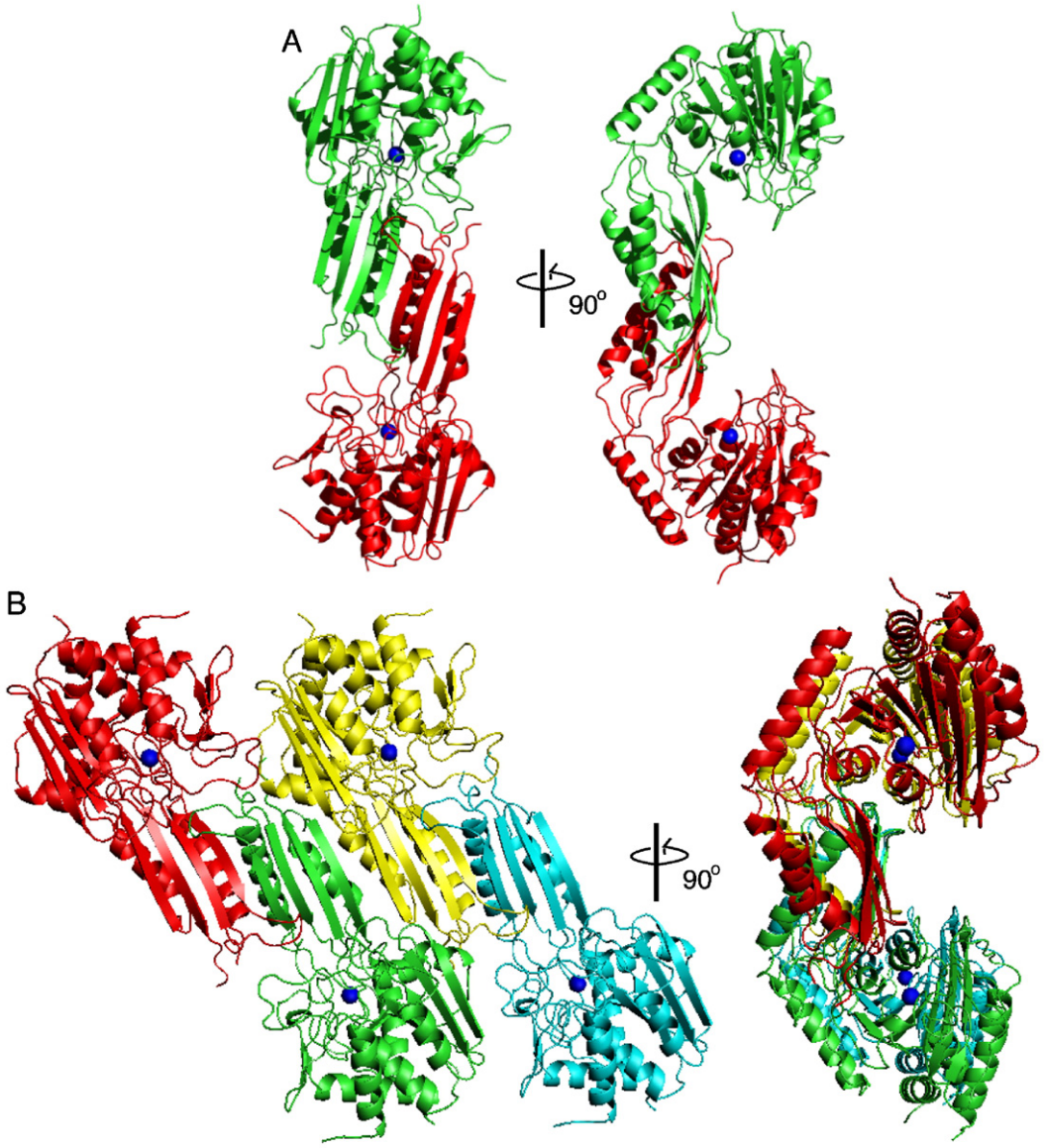

Fig. 3. Quaternary structure of ACDase. (A) Ribbon diagram of the dimer in two different orientations. (B) Ribbon diagrams of the possible tetramer in different orientations. The Co(II) ion in the active site is shown as a ball. The figures were drawn with Pymol [29].

structure. After thrombin digestion, three residues, Gly–Ser–His, that are not part of the wild-type protein precede the Met residue at the *N*-terminus of the protein. The Gly and Ser residues are not visible in the electron density map, but there is electron density for the His, which was included in the model. The density for residues 180–185 and the C-terminal His365 is too weak to be modeled. All other residues were well defined by the electron density and refined to an average temperature factor $B=25.1$ Å^2. One non-proline *cis*-peptide bond was found between active site residues Asp103 and Ile104. Equivalent *cis*-peptide bonds were also identified in the structures of succinyldiaminopimelate desuccinylase from *N. meningitidis mc58* between Asp101 and Met102 [17], carboxypeptidase G2 from *Pseudomonas* sp. between Asp141 and Asp142 [18], and *A. proteolytica* aminopeptidase between Asp117 and Asp118 [19]. Conservation of this energetically unfavorable conformation indicates that these *cis*-peptide bonds have an important functional role. The metal-free and Co(II)-bound structures are similar to each other with an r.m.s. difference of 0.114 Å for all 360 equivalent Cα atoms, indicating that no conformational change occurs upon Co(II) binding. The subsequent results and discussion are based on the Co(II)-bound structure unless otherwise indicated.

Sequence alignment of *X. campestris* ACDase, *E. coli* AODase, *N. meningitidis* succinyl diaminopimelate desuccinylase and *Pseudomonas* sp. strain RS-16 carboxypeptidase G2 with the secondary structural elements are shown in Fig. 1. The ribbon diagram of the ACDase monomer consisting of two domains is shown in Fig. 2A. The general fold is closely related to succinyldiaminopimelate desuccinylase from *N. meningitidis mc58* [17] and carboxypeptidase G2 from *Pseudomonas* sp. [18] (Fig. 2B and C), as the sequence comparison predicted. However, the structural details for the loop regions and helix positions are significantly different, especially for the position of helix H7.

The catalytic domain consists of residues 1–166 and 286–365 from the N and C termini, respectively. Its fold is similar to those of other exopeptidases such as *A. proteolytica* aminopeptidase [19], bovine lens leucine aminopeptidase [20], and carboxypeptidase A [21]. A strongly twisted six-stranded β sheet (arranged as B12↑, B7↑, B3↑, B6↑, B2↓, B1↑) is sandwiched between α helices (H1, H2, H3 and H10 on one side; H4, H8, H9 on another side) to form the hydrophobic core and a second short three-stranded β sheet (arranged as B13↓, B5↑, B4↓) is located on the surface of the molecule. A helix (H7) that links the two domains is approximately perpendicular to the other β sheets and α helices.

The second domain (residues 167–285), which forms the dimer interface, folds into a four-stranded anti-parallel β sheet (arranged as B9↑, B10↓, B8↑, B11↓) flanked on one side by two α helices (H5 and H6)(Fig. 2A). As noted previously [18], this domain is topologically similar to the RNA-binding domains of other proteins such as phenylalanyl-tRNA synthetase [22], and acylphosphatase [23].

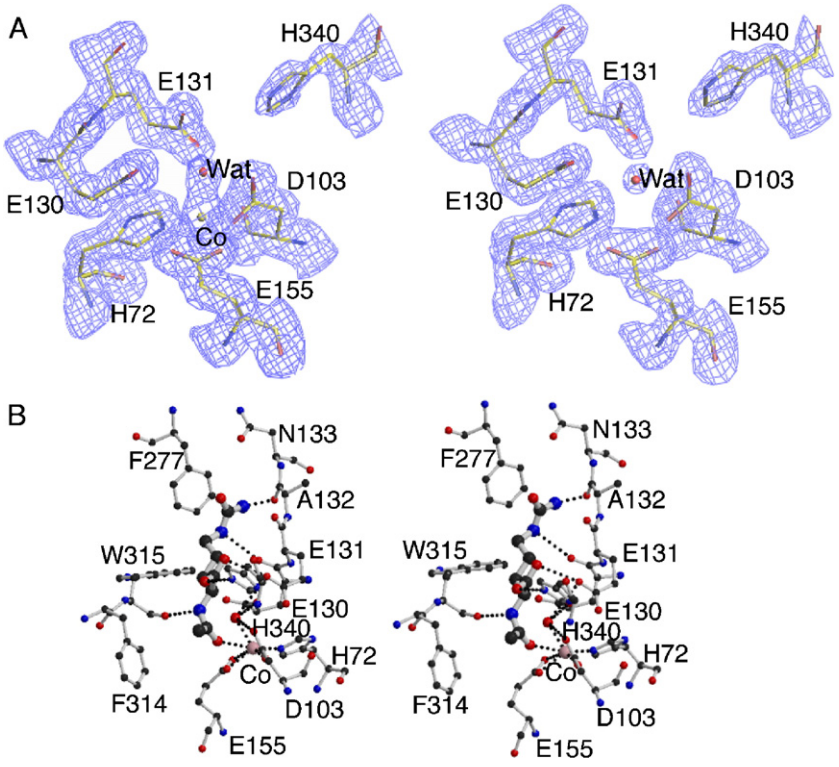

Fig. 4. Active site and substrate binding model. (A) Contours of the electron density maps ($2F_o$–F_c) (1.3σ shown in blue cage) at the active site of the Co(II)-bound structure (left) and the Co(II)-free structure (right). The final refined positions are superimposed and represented as colored sticks and balls. (B) Stereo view of the substrate binding model. Glu131 and His340 from a potential second metal binding site are proposed to be involved in binding the substrate. The figures were drawn with O [14], MOLSCRIPT [27] and Raster3D [28].

3.2. Quaternary structure

The dimer interface involves hydrophobic interactions between helices and hydrogen bonding between two β strands which form a continuous β sheet across the dimer (Fig. 3A). The monomers are related to each other by exact two-fold symmetry and the dimers are also related to each other via the second domain by two-fold crystallographic axes across the crystal (Fig. 3B), implying that higher oligomers may form in solution, as is the case for *E. coli* AODase, which exists in solution as both tetramers and octamers [3].

Interactions between monomers within the biologically relevant dimer are much stronger than those at the dimer–dimer interface. However, since the active site of ACDase is far from the dimer interface, dimerization may not be catalytically essential.

The structure of the dimer is similar to those of succinyldiaminopimelate desuccinylase from *N. meningitidis mc58* [17] and carboxypeptidase G2 from *Pseudomonas* sp. [18]. However, the dimers of carboxypeptidase G2 further interact face to face to form a tetramer.

3.3. Metal binding site

Although acetylases sometimes bind to more than one metal ion, only a single Co(II) binding site was identified in ACDase. It is located at the surface of the catalytic domain in a V-shaped cavity between the two domains (Fig. 2A) and is coordinated by NE2 of His72, the carboxylate O atoms of Asp103 and Glu155, and one water molecule (Fig. 4A). The coordination geometry is consistent with the five-coordinate environment suggested by the EPR spectrum of *E. coli* AODase [3].

3.4. Substrate binding

Although the structure of ACDase with a substrate or substrate analog bound has not yet been determined, substrate binding can be modeled using closely related structures such as succinyldiaminopimelate desuccinylase from *N. meningitidis mc58* (PDB ID: 1VGY) [17], carboxypeptidase G2 from a *Pseudomonas* sp. (PDB ID: 1CG2) [18], and aminopeptidase from *A. proteolytica* [19]. The model shown in Fig. 4B indicates that the substrate binding site involves residues of the second metal binding site as in *E. coli* aminopeptidase P [24] and UDP-3-*O*-((*R*)-3-hydroxymyristoyl)-*N*-acetylglucosamine deacetylase [25]. Glu131 and His340, which are part of a second metal binding site in *N. meningitidis mc58* succinyldiaminopimelate desuccinylase and *Pseudomonas* sp. carboxypeptidase G2, appear to interact with the carboxyl group of the substrate while the carbonyl O atom of Trp315 hydrogen bonds to the imino N atom of the substrate. The methyl group of the substrate interacts with Phe314 and Ile336, while the side chain of the substrate is enclosed by the hydrophobic side-chains of Trp315 and Phe277 on one side, and hydrophilic groups such as the carbonyl O atoms of Glu130, Glu131 and Ala132 on the other side.

Comparison of this model with related structures accounts for their known substrate specificity. Both the shape and hydrophobicity of the side-chain pocket define substrate specificity. For example, since the pocket for the side chain of the substrate is half hydrophobic and half hydrophilic, other acetylated amino acids with hydrophobic side-chains should be substrates, and *E. coli* AODase, which has many similarities to ACDase, has recently been shown to deacetylate *N*-acetyl-L-methionine [2]. In the carboxypeptidase G2 structure, the active site pocket is much wider enabling its much bulkier substrates, folate or methotrexate, to bind, and Arg324 is positioned so that it can bind the carboxyl group of the side chain, as suggested previously [17]. At the other end of the binding pocket, Trp315 and Phe277 in *X. campestris* ACDase are replaced by Thr326 and Arg330 in *N. meningitidis mc58* succinyldiaminopimelate desuccinylase, enabling the side chain of Arg330 to be involved in binding the carboxyl side chain of diaminopimelate. Phe314 and the equivalent residues in related enzymes are likely to play critical roles in discriminating between acetylated and succinylated substrates. In ACDase, Phe314 would block binding of the succinyl group, whereas in *N. meningitidis mc58* succinyldiaminopimelate desuccinylase, the equivalent residue is Gly325, which enables the bulkier succinyl group to access the active side. In addition, Arg179 is oriented towards the active site and interacts with the succinyl group.

3.5. Mechanism

A model of the catalytic mechanism which is consistent with the structure is shown in Fig. 5. This model is similar to those of mononuclear metalloproteases, in that the metal ion interacts with the carbonyl group to polarize the amide bond, while a Glu

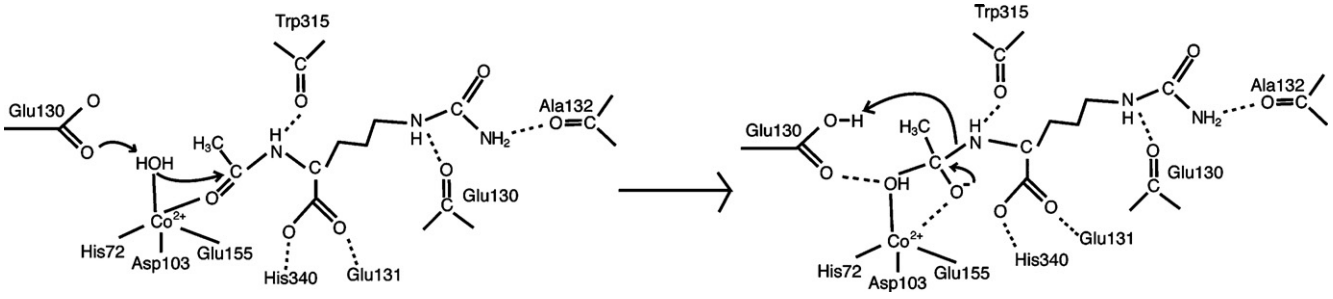

Fig. 5. Schematic drawing of the substrate binding model using the second metal-binding residues, Glu131 and His340, to bind the substrate, and the proposed model of the catalytic mechanism with Glu130 as a single bifunctional general acid–base catalyst.

residue participates as a bifunctional general acid–base catalyst. In this model, the attacking water molecule is Wat94, which is coordinated to the Co(II) ion bound at the active site. Glu130 functions as a general acid–base catalyst, activating Wat94, while the metal ion interacts with the acetyl group to polarize the amide bond. The departing amino group is then protonated by Glu130, leading to the breakdown of the tetrahedral intermediate. While mechanisms involving both a single bifunctional general acid–base catalyst and two general acid–base catalysts have been proposed for deacetylases [8], the structure of ACDase is consistent with a requirement for only one. Further experiments will be required to determine if this is indeed correct.

4. Conclusion

We present here the first structure of a novel ACDase from *X. campestris*. The monomer has a two-domain fold consisting of a catalytic domain and a dimerization domain similar to those of *Pseudomonas* sp. carboxypeptidase G2 and *N. meningitidis* succinyl diaminopimelate desuccinylase. Within the active site, only one Co(II) binding site was observed in the absence of substrate analog. Models for substrate binding and the catalytic mechanism based on structural comparisons with other related enzymes are proposed. The model of the catalytic mechanism suggests that ACDase and AODase, which is closely related, require only a single metal ion for substrate binding and the catalytic reaction. Glu130 is proposed to function as a bifunctional general acid–base catalyst. This structure provides a starting point for designing specific non-toxic inhibitors of the growth of plant pathogens with this unique enzyme in their arginine biosynthetic pathway.

Acknowledgments

This work was supported by Public Health Service grant DK-47870 (MT) and DK-067935 (DS) from the National Institute of Diabetes, Digestive and Kidney Diseases and HD 32652 from the National Institute of Child Health and Human Development. We thank Dr. David Davies for facilitating the use of the diffraction equipment in the Molecular Structure Section of the National Institute of Health and Dr. Fred Dyda for help in data collection. We also thank Drs. Alexei Soares and Stu Myers for their assistance during data collection at beamline X26C and X12B at Brookhaven National Laboratory. This facility is supported by the United States Department of Energy Offices of Health and Environmental Research and of Energy Sciences, and by the National Science Foundation.

References

[1] R. Cunin, N. Glansdorff, A. Pierard, V. Stalon, Biosynthesis and metabolism of arginine in bacteria, Microbiol. Rev. 50 (1986) 314–352.
[2] F. Javid-Majd, J.S. Blanchard, Mechanistic analysis of the *argE*-encoded *N*-acetylornithine deacetylase, Biochemistry 39 (2000) 1285–1293.
[3] W.C. McGregor, S.I. Swierczek, B. Bennett, R.C. Holz, argE-encoded *N*-Acetyl-L-ornithine deacetylase from *Escherichia coli* contains a dinuclear metalloactive site, J. Am. Chem. Soc. 127 (2005) 14100–14107.
[4] T. Meinnel, E. Schmit, Y. Mechulam, S. Blanquet, Structural and biochemical characterization of the *Escherichia coli* argE gene product, J. Bacteriol. 174 (1992) 2323–2331.
[5] D. Shi, H. Morizono, X. Yu, L. Roth, L. Caldovic, N.M. Allewell, M.H. Malamy, M. Tuchman, Crystal structure of *N*-acetylornithine transcarbamoylase from *Xanthomonas campestris*: a novel enzyme in a new arginine biosynthetic pathway found in several eubacteria, J. Biol. Chem. 280 (2005) 14366–14369.
[6] H. Morizono, J. Cabrera-Luque, D. Shi, R. Gallegos, S. Yamaguchi, X. Yu, N.M. Allewell, M.H. Malamy, M. Tuchman, Acetylornithine transcarbamylase: a novel enzyme in arginine biosynthesis, J. Bacteriol. 188 (2006) 2974–2982.
[7] D. Shi, X. Yu, L. Roth, H. Morizono, Y. Hathout, N.M. Allewell, M. Tuchman, Expression, purification, crystallization and preliminary X-ray crystallographic studies of a novel acetylcitrulline deacetylase from *Xanthomonas campestris*, Acta Crystallogr., F 61 (2005) 676–679.
[8] M. Hernick, C.A. Fierke, Zinc hydrolases: the mechanisms of zinc-dependent deacetylases, Arch. Biochem. Biophys. 433 (2005) 71–84.
[9] B.W. Matthews, Determination of molecular weight from protein crystals, J. Mol. Biol. 82 (1974) 513–526.
[10] Z. Otwinowski, W. Minor, Processing of X-ray diffraction data collected in oscillation mode, Methods Enzymol. 276 (1997) 307–326.
[11] Collaborative Computational Project, Number 4, The CCP4 suite: programs for protein crystallography, Acta Crystallogr., D 50 (1994) 760–763.
[12] T.C. Terwilliger, J. Berendzen, Automated MAD and MIR structure solution, Acta Crystallogr., D 55 (1999) 849–861.
[13] T.C. Terwilliger, SOLVE and RESOLVE: automated structure solution, density modification and model building, J. Synchrotron Radiat. 11 (2004) 49–52.
[14] T.A. Jones, J.Y. Zou, S.W. Cowan, M. Kjeldgaard, Improved methods for building protein models in electron density maps and location of errors in these model, Acta Crystallogr., A 47 (1991) 110–119.
[15] A.T. Brünger, P.D. Adams, G.M. Clore, W.L. DeLano, P. Gros, R.W. Crosse-Kunstleve, J.S. Jiang, J. Kuszewski, M. Nilges, N.S. Pannu, R.J. Read, L. Rice, M.T. Simonson, G.L. Warren, Crystallography and NMR system: a new software suite for macromolecular structure determination, Acta Crystallogr., D 54 (1998) 905–921.
[16] R.A. Laskowski, M.W. MacArthur, D.S. Moss, J.M. Thornton, PROCHECK—A program to check the stereochemical quality of protein structures, J. Appl. Crystallogr. 26 (1993) 283–291.
[17] J. Badger, J.M. Sauder, J.M. Adams, S. Antonysamy, K. Bain, M.G. Bergseid, S.G. Buchanan, M.D. Buchanan, Y. Batiyenko, J.A. Christopher, S. Emtage, A. Eroshkina, I. Feil, E.B. Furlong, K.S. Gajiwala, X. Gao, D. He, J. Hendle, A. Huber, K. Hoda, P. Kearins, C. Kissinger, B. Laubert, H.A. Lewis, J. Lin, K. Loomis, D. Lorimer, G. Louie, M. Maletic, C.D. Marsh, I. Miller, J. Molinari, H.J. Muller-Dieckmann, J.M. Newman, B.W. Noland, B. Pagarigan, F. Park, T.S. Peat, K.W. Post, S. Radojicic, A. Ramos, R. Romero, M.E. Rutter, W.E. Sanderson, K.D. Schwinn, J. Tresser, J. Winhoven, T.A. Wright, L. Wu, J. Xu, T.J. Harris, Structural analysis of a set of proteins resulting from a bacterial genomics project, Proteins 60 (2005) 787–796.
[18] S. Rowsell, R.A. Pauptit, A.D. Tucker, R.G. Melton, D.M. Blow, P. Brick, Crystal structure of carboxypeptidase G2, a bacterial enzyme with applications in cancer therapy, Structure 5 (1997) 337–347.
[19] B. Chevrier, H. D'Orchymont, C. Schalk, C. Tarnus, D. Moras, The structure of the *Aeromonas proteolytica* aminopeptidase complexed with a hydroxamate inhibitor. Involvement in catalysis of Glu151 and two zinc ions of the co-catalytic unit, Eur. J. Biochem. 237 (1996) 393–398.
[20] S.K. Burley, P.R. David, A. Taylor, W.N. Lipscomb, Molecular structure of leucine aminopeptidase at 2.7-A resolution, Proc. Natl. Acad. Sci. U. S. A. 87 (1990) 6878–6882.
[21] F.A. Quiocho, W.N. Lipscomb, Carboxypeptidase A: a protein and an enzyme, Adv. Protein Chem. 25 (1971) 1–78.
[22] L. Mosyak, L. Reshetnikova, Y. Goldgur, M. Delarue, M.G. Safro, Structure of phenylalanyl-tRNA synthetase from *Thermus thermophilus*, Nat. Struct. Biol. 2 (1995) 537–547.

[23] V. Saudek, M.R. Wormald, R.J. Williams, J. Boyd, M. Stefani, G. Ramponi, Identification and description of beta-structure in horse muscle acylphosphatase by nuclear magnetic resonance spectroscopy, J. Mol. Biol. 207 (1989) 405–415.
[24] S.C. Graham, C.S. Bond, H.C. Freeman, J.M. Guss, Structural and functional implications of metal ion selection in aminopeptidase p, a metalloprotease with a dinuclear metal center, Biochemistry 44 (2005) 13820–13836.
[25] M. Hernick, H.A. Gennadios, D.A. Whittington, K.M. Rusche, D.W. Christianson, C.A. Fierke, UDP-3-*O*-((*R*)-3-hydroxymyristoyl)-*N*-acetylglucosamine deacetylase functions through a general acid–base catalyst pair mechanism, J. Biol. Chem. 280 (2005) 16969–16978.
[26] G.J. Barton, ALSCRIPT: a tool to format multiple sequence alignments, Protein Eng. 6 (1993) 37–40.
[27] P.J. Kraulis, MOLSCRIPT: a program to produce both detailed and schematic plots of protein structures, J. Appl. Crystallogr. 24 (1991) 946–950.
[28] E.A. Merritt, M.E. Murphy, Raster3D Version 2.0. A program for photorealistic molecular graphics, Acta Crystallogr., D 50 (1994) 869–873.
[29] W.L. DeLano, The PyMOL Molecular Graphics System, http://www.pymol.org, 2002.